Evaluating GAN-Based RGB Image Translation Using ALOS-2 Polarimetric SAR Data for Agricultural Monitoring

Hirofumi Shimaoka[1], Kan-ichiro Mochizuki[2] and Rei Sonobe[1]

[1] Graduate School of Integrated Science and Technology, Shizuoka University, Shizuoka, Japan.
[2] PASCO Corporation, Tokyo, Japan

Keywords: ALOS-2/PALSAR-2, PlanetScope, Polarimetric SAR, Agricultural Monitoring

Abstract

Synthetic Aperture Radar (SAR) offers an all-weather alternative, and recent advances in deep generative models provide opportunities to reconstruct optical-like imagery directly from SAR data. In this study, we conduct a comparative evaluation of multiple generative adversarial network (GAN) architectures for translating SAR data into realistic red, green and blue (RGB) imagery in agricultural landscapes. The models were trained using ALOS-2/PALSAR-2 quad-polarimetric (quad-pol) data. A distinctive feature of our work is the evaluation of not only backscatter coefficients (Gamma nought) but also polarimetric parameters derived from quad-pol decompositions, including the generalised Freeman–Durden, H/A/Alpha, and Yamaguchi four-component methods. The comparative results show that paired image-to-image translation frameworks consistently outperform unpaired approaches. In particular, paired methods such as feature-guiding GAN and pix2pixHD, achieved high similarity to PlanetScope reference imagery, with mean structural similarity index values exceeding 0.98 across all SAR inputs. In contrast, unpaired approaches demonstrated more variable performance depending on the input features. Notably, PUT showed significant improvement when H/A/Alpha or Yamaguchi decompositions were used, whereas Freeman–Durden produced results comparable to Gamma nought. The performance gap between paired and unpaired frameworks was most evident in heterogeneous landscapes, such as areas with adjacent grasslands and forests. These findings demonstrate the effectiveness of GAN-based translation from polarimetric SAR to RGB imagery for agricultural monitoring. The integration of polarimetric information adds value to unpaired learning schemes, and the ability to generate optical-like imagery under challenging observation conditions has strong potential for practical use in crop monitoring and assessment.

1. Introduction

Synthetic Aperture Radar (SAR) imagery has become an essential tool for agricultural monitoring because of its ability to capture surface characteristics irrespective of weather and illumination conditions (McNairn and Shang, 2016; Sonobe, 2019a, 2019b; Sonobe et al., 2015; Sonobe and Tani, 2009). The Japanese ALOS-2/PALSAR-2 satellite provides high-resolution quad-polarimetric (quad-pol) SAR data, enabling detailed analysis of scattering mechanisms from agricultural fields (Plank et al., 2017; Rosenqvist et al., 2014). However, interpreting SAR imagery is inherently challenging because the recorded signals represent complex microwave scattering interactions between the radar waves and surface structures, vegetation, and moisture conditions, rather than direct optical reflectance. As a result, the appearance of SAR images is often influenced by factors such as surface roughness, dielectric properties, and sensor viewing geometry, which makes the physical meaning of image brightness and texture less intuitive for human interpretation (Di Martino et al., 2012). Generating intuitive and visually interpretable red-green-blue (RGB) images from SAR data can significantly enhance usability by bridging the gap between radar backscatter signals and human visual perception (Sonobe et al., 2025, 2024). This process enables stakeholders such as farmers, policymakers, and remote-sensing analysts to interpret crop growth, soil moisture, and field conditions with greater ease. By transforming polarimetric SAR signals into RGB representations, information-rich data can be incorporated into user-friendly visualisation tools, thereby expanding the potential benefits of SAR data beyond specialist communities. In particular, agricultural areas – where monitoring crop type, biomass, and soil conditions is critical – stand to benefit greatly from improved visualisation of polarimetric information (Lopez-Sanchez and David Ballester-Berman, 2009; McNairn and Brisco, 2004; Wiseman et al., 2014). Thus, developing robust methods for translating ALOS-2/PALSAR-2 quad-pol data into colour images is of both scientific and practical importance.

Recent advances in deep learning have led to remarkable progress in image-to-image translation tasks, with generative adversarial networks (GANs) emerging as one of the most powerful frameworks (Chen and Jia, 2021; Goodfellow et al., 2020; Kamil and Shaikh, 2019). GANs learn mappings between two domains by training a generator to produce realistic outputs and a discriminator to distinguish generated images from real ones (Dash et al., 2024; Goodfellow et al., 2020). Through adversarial training, GANs can capture complex distributions and produce high-quality, visually convincing results. Several notable GAN architectures have been proposed to advance image translation across domains (Pang et al., 2022). Attention GAN (AttenGAN) incorporates attention mechanisms to better align visual features with semantic content, enhancing fine-grained detail generation (Tang et al., 2023, 2019). Cycle-consistent GAN (CycleGAN) introduced the concept of cycle-consistency, enabling unpaired image-to-image translation and achieving high influence in cross-domain applications (Zhu et al., 2017). Feature-guiding GAN (FGGAN) emphasises detailed representation learning, making it well-suited to tasks where structural fidelity is crucial (Yang et al., 2020). pix2pixHD extends the conditional GAN framework to generate high-resolution images, producing sharper and more realistic outputs for real-world applications (Wang et al., 2018). More recently, methods such as exploring negatives in contrastive learning for unpaired image-to-image translation (PUT) have advanced the field by introducing contrastive learning, which improves robustness and translation accuracy when training data are limited or unpaired (Lin et al., 2022). Collectively, these GAN-based models represent the state of the art in image translation,

This contribution has been peer-reviewed. The double-blind peer-review was conducted on the basis of the full paper.
https://doi.org/10.5194/isprs-annals-XI-3-2026-797-2026 | © Author(s) 2026. CC BY 4.0 License.

demonstrating strong potential for SAR-to-RGB conversion tasks where data domains differ significantly in both visual and statistical properties. Their success in natural image domains highlights their promise for bridging the interpretability gap between SAR signals and human-friendly colour visualisations.

Traditionally, the generation of RGB-like images from SAR data has relied heavily on backscatter coefficients such as sigma nought or gamma nought. While backscatter provides essential information on surface roughness and dielectric properties, it does not fully exploit the richness of quad-pol SAR data. To address this limitation, a range of polarimetric decomposition techniques have been developed to extract physically meaningful parameters that characterise scattering mechanisms more effectively. For example, the generalised Freeman–Durden decomposition offers a flexible framework for separating surface, double-bounce, and volume scattering components (Cloude, 2010). The H/A/Alpha decomposition provides eigenvalue-based parameters that quantify entropy, anisotropy, and scattering angle, offering deeper insights into scattering diversity (Lee and Pottier, 2009). Yamaguchi’s four-component decomposition further refines scattering interpretation by including helix scattering in addition to surface, double-bounce, and volume contributions (Yamaguchi et al., 2005). These polarimetric parameters extend beyond simple backscatter intensities to provide richer descriptions of scattering processes, which can be particularly valuable for distinguishing agricultural features such as crop structure, growth stage, and field conditions. Incorporating these parameters into SAR-to-RGB translation frameworks may enable the generation of colour images that are not only visually intuitive but also more informative, because they reflect the underlying physical scattering processes.

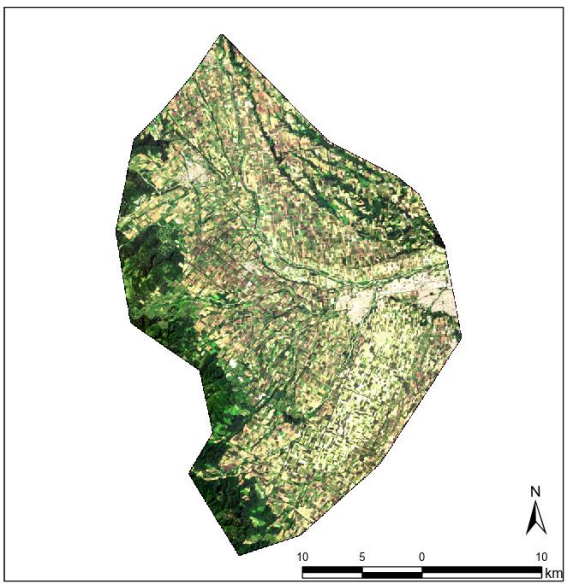

Figure 1. Study area. The study area is located in the western part of the Tokachi Plain in Hokkaido, Japan, a major agricultural region characterised by large-scale croplands and relatively flat terrain with elevations ranging from approximately 50 to 230 m above sea level.

The objective of this study is to investigate the potential of combining ALOS-2/PALSAR-2 quad-pol information with GAN-based image translation models to generate RGB images. By systematically comparing RGB images generated from both backscatter coefficients and various polarimetric parameters, this research aims to identify the optimal combination of input features and GAN architectures. The ultimate aim is to enhance both the interpretability and the practical value of SAR data in agricultural applications, thereby supporting more effective and user-friendly remote-sensing solutions.

2. Methodology

The study area is an agricultural region located in the western part of the Tokachi Plain, Hokkaido, Japan, at elevations ranging from 50 to 230 metres (Figure 1).

For SAR imagery, quad-pol data acquired by ALOS-2/PALSAR-2 in SM2 observation mode on 22 June 2024 were used. The data were provided at Level 1.1 and orthorectified using ellipsoidal height based on the Earth Gravitational Model 2008. They were then converted into backscatter coefficient (γ^0) images with a pixel resolution of 3 m, using cubic convolution resampling. In addition to backscatter coefficients, polarimetric components were derived using several decomposition methods: the generalised Freeman–Durden decomposition, which provides a flexible framework for separating dominant scattering mechanisms; the H/A/Alpha decomposition, which extracts entropy, anisotropy, and scattering angle to characterise scattering randomness and target orientation; and Yamaguchi’s four-component decomposition, which extends conventional models by incorporating helix scattering in addition to surface, double-bounce, and volume components. These decompositions were used to generate corresponding images that enriched the representation of scattering mechanisms beyond simple backscatter intensity.

For optical imagery, SuperDove satellite data acquired by Planet Labs Netherlands B.V.’s PSB.SD sensor on 29 June 2024 were used. While PSB.SD offers eight spectral bands – Coastal Blue, Green I, Yellow, and Red Edge in addition to the four conventional PS2.SD bands (red, green, blue, and NIR) – only the red, green, and blue bands were used to generate composite colour images in this study. The data were provided at Level 3B with a pixel resolution of 3 m.

GAN-based image translation has recently attracted considerable attention for SAR-to-optical conversion because it can learn complex nonlinear relationships between radar backscatter patterns and optical reflectance. Previous studies have demonstrated that both paired and unpaired GAN frameworks can generate visually plausible optical-like imagery from SAR data, but their relative performance and sensitivity to SAR feature representations remain insufficiently understood. Motivated by these studies, this research adopts a comparative experimental framework to systematically evaluate representative GAN architectures under identical conditions.

The GAN models were implemented in Google Colaboratory. The study area was divided into 1,183 patches of 256 × 256 pixels. Of these, 111 patches were randomly selected for evaluation, while the remaining patches were used to tune the parameters of each GAN model. After parameter tuning, the trained generators were applied to the 111 evaluation patches to generate synthetic images.

To ensure a fair comparison, all models were trained using the same dataset, patch size, training?evaluation split, and computational environment. Hyperparameters were tuned using the same training subset, and the final evaluation was conducted using the identical set of held-out patches. Five representative

Table 1. GAN architectures used in this study and their source websites.

Architecture	URL
AttentionGAN-v2 (AttenGAN)	https://github.com/Ha0Tang/AttentionGAN
Cycle-Consistent Generative Adversarial Networks (CycleGAN)	https://github.com/ junyanz/pytorch-CycleGAN-and-pix2pix
Feature-Guiding Generative Adversarial Networks (FGGAN)	https://github.com/JessieZ96/SAR-to-Optical
High-Resolution Image Synthesis and Semantic Manipulation with Conditional GANs (pix2pixHD)	https://github.com/NVIDIA/pix2pixHD
Exploring Negatives in Contrastive Learning for Unpaired Image-to-Image Translation (PUT)	https://github.com/YupeiLin2388/Exploring-Negatives-in-Contrastive-Learning-for-Unpaired-Image-to-Image-Translation

GAN-based models were selected for comparison. The selection criteria were based on their widespread use in image-to-image translation tasks, their relevance to SAR-to-optical conversion reported in previous studies, and their ability to represent both paired and unpaired learning paradigms. This allows the comparative framework to capture differences in learning strategies and their impact on SAR image translation performance. The following five GAN-based models were used to generate RGB images from SAR data:

AttenGAN (Tang et al., 2023, 2019)
This model incorporates an attention mechanism based on spatial features to generate images that faithfully preserve the structure and shape of target regions. It integrates multi-scale features and attention maps to produce localised and semantically consistent translations.

CycleGAN (Zhu et al., 2017)
This widely used model for unpaired image translation introduces cycle-consistency loss, ensuring that forward and backward transformations between domains yield consistent results.

FGGAN (Yang et al., 2020)
This model incorporates a feature guidance module that extracts and enhances low-level visual features (e.g., edges and textures) to improve structural coherence and visual clarity. It is particularly effective for SAR-to-optical translation, where physical differences between domains are especially evident.

High-Resolution Image Synthesis and Semantic Manipulation with Conditional GANs (pix2pixHD) (Wang et al., 2018)
This conditional GAN is designed for high-resolution image synthesis. It combines multi-scale generators and discriminators to produce high-quality results with fine-grained detail.

Exploring Negatives in Contrastive Learning for PUT (Lin et al., 2022)
This model integrates contrastive learning into the GAN framework. By learning distances between positive and negative pairs, it enhances feature consistency even in the absence of paired data. This approach allows the model to learn semantically meaningful correspondences and perform effectively in complex domain translation tasks.

Synthetic colour images were generated using Google Colaboratory with a Tesla T4 GPU. The relevant Python code was downloaded from the repositories listed in Table 1.

All models were executed under the same hardware environment and training settings to minimise implementation-related differences and ensure comparability of the results.

The quality of the generated images was evaluated using the structural
similarity index measure (SSIM) (Wang et al., 2004). SSIM is a widely used metric for assessing similarity between two images.

Unlike traditional measures such as mean squared error or peak signal-to-noise ratio, which compare pixel-by-pixel differences, SSIM is designed to model how human vision perceives image quality. It recognises that the human eye is highly sensitive to structural information in a scene, meaning that patterns of edges, textures, and contrast are more important than exact pixel values. To capture this, SSIM evaluates similarity based on three main components: luminance, contrast, and structure. The luminance comparison checks whether the average brightness levels of two images are consistent, the contrast comparison examines the variations in intensity, and the structure comparison captures how well the normalised patterns of local details align. By combining these factors, this combined metric produces a value between –1 and 1, where 1 represents perfect similarity, 0 indicates no similarity, and negative values imply structural dissimilarity.

3. Results

Figure 2 illustrates the distribution of SSIM values across different GAN architectures for each spectral band (red, green, blue) and SAR-derived datasets (G: Gamma nought, F: generalised Freeman–Durden decomposition, H: H/A/Alpha decomposition, Y: Yamaguchi's four-component decomposition). The analysis of SSIM statistics across SAR datasets, GAN architectures, and spectral bands reveals distinct and meaningful performance patterns. As shown in Figure 2, the boxplot distributions allow direct comparison of median, quartile ranges, and outliers across all experimental settings, providing a quantitative basis for the following analysis.

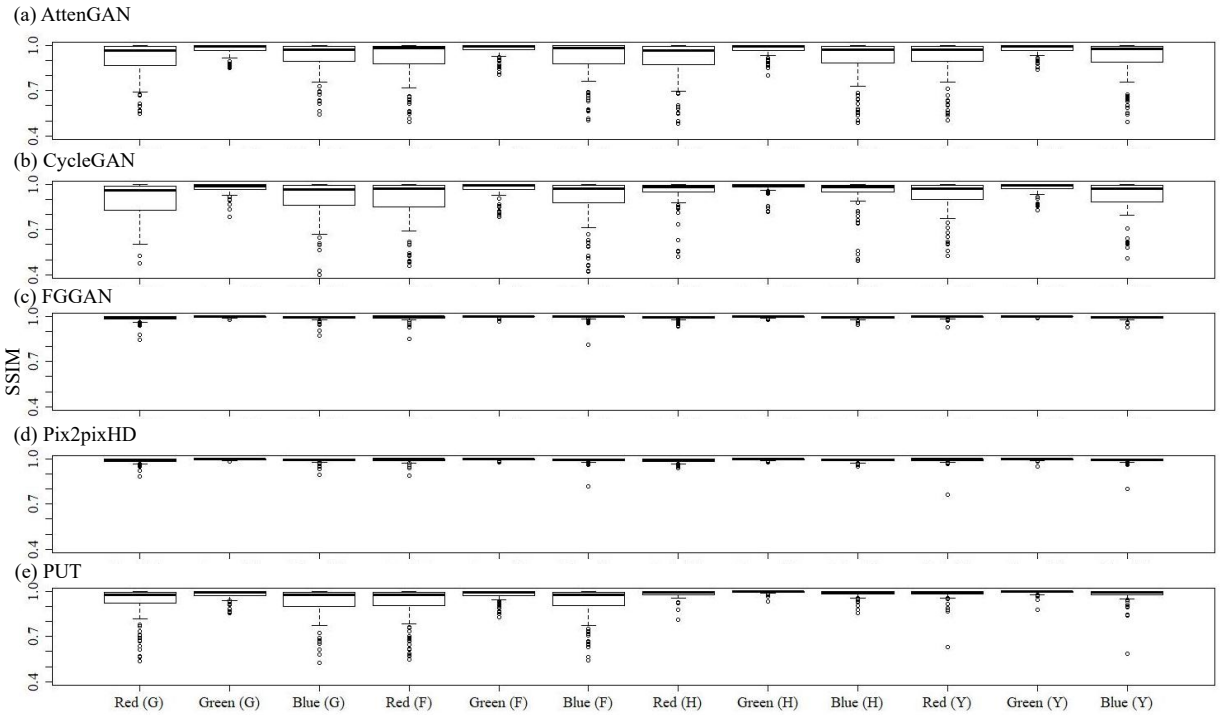

Figure 2. Distribution of structural similarity index measure (SSIM) values across different GAN architectures for each spectral band (red, green, blue) and SAR-derived datasets (G: Gamma nought; F: Generalised Freeman–Durden decomposition; H: H/A/Alpha decomposition; Y: Yamaguchi’s four-component decomposition).

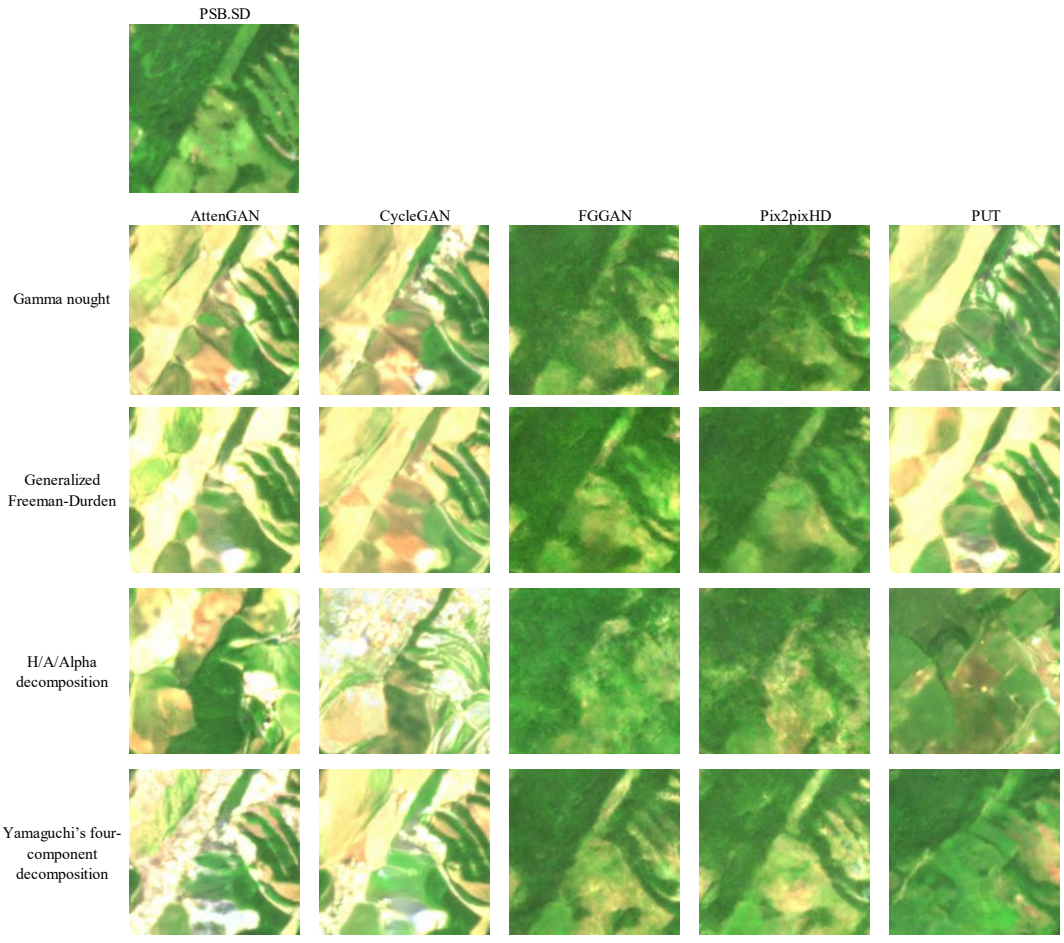

Figure 3. PSB.SD image and generated images.

This contribution has been peer-reviewed. The double-blind peer-review was conducted on the basis of the full paper.
https://doi.org/10.5194/isprs-annals-XI-3-2026-797-2026 | © Author(s) 2026. CC BY 4.0 License.

3.1 SAR Data

The analysis of SSIM values across different SAR datasets reveals notable differences in reconstruction quality. As illustrated in Figure 2, the Gamma nought dataset shows a wider distribution of SSIM values compared with the polarimetric decomposition datasets. For the Gamma nought dataset, overall performance remains satisfactory, with median and mean SSIM values consistently high; however, this dataset shows comparatively lower minimum values. This pattern is visible in Figure 2 as a longer lower whisker and several lower-value observations, indicating that although most reconstructions are reliable, there are occasional cases where the model struggles to reproduce fine structural details, resulting in a broader distribution of SSIM values.

By contrast, the decomposed polarimetric features provide more robust performance. In Figure 2, the boxplots corresponding to the generalised Freeman-Durden and H/A/Alpha datasets show consistently higher median SSIM values and narrower interquartile ranges. For example, both the generalised Freeman–Durden and H/A/Alpha datasets consistently achieve higher median and mean SSIM values, often exceeding 0.97 or even 0.98, suggesting that the physical scattering information encoded in these decompositions significantly contributes to preserving spatial and textural fidelity in the generated images.

The Yamaguchi decomposition also performs well, producing SSIM scores comparable to, or slightly below, the best-performing datasets. This trend can also be observed in Figure 2, where the Yamaguchi-based inputs maintain relatively high medians while showing slightly greater variability than the Freeman-Durden and H/A/Alpha decompositions. Importantly, the variation across statistical measures is smaller for decomposed datasets compared to Gamma nought, highlighting the stability of these inputs. The tighter distributions in Figure 2 therefore indicate that polarimetric decomposition features provide more stable inputs for the GAN models.

Taken together, these findings suggest that polarimetric decompositions are advantageous for image-to-image translation tasks using GANs because they encode richer scattering mechanisms that enable structurally faithful reconstructions across diverse spectral bands and generative models.

3.2 GAN Models

A comparison of GAN architectures reveals clear differences in their ability to preserve structural similarity. As shown in Figure 2, the boxplots for FGGAN and pix2pixHD are consistently positioned at the upper end of the SSIM distribution across SAR datasets and spectral bands. FGGAN and pix2pixHD consistently achieve the highest SSIM values across SAR datasets and bands, with median and mean values frequently exceeding 0.99. This indicates that these models excel at capturing fine-scale spatial information, resulting in faithful reconstructions with minimal loss of detail. The narrow interquartile ranges observed in Figure 2 further demonstrate the stability of these two models, as the difference between minimum and maximum SSIM values remains relatively small across different datasets.

By contrast, AttenGAN and CycleGAN exhibit slightly weaker performance. In Figure 2, their boxplots are positioned slightly lower than those of FGGAN and pix2pixHD and show greater spread, characterised by lower median SSIM values and greater variability. Although these models still achieve relatively high mean scores, often between 0.97 and 0.98, their performance is less consistent, suggesting reduced generalisation across data types and spectral bands. PUT performs the weakest overall, as evidenced by its substantially lower mean SSIM values compared to the other models. The wider standard deviations in PUT-generated results further indicate instability, implying it struggles to reproduce fine details reliably and maintain structural integrity. This ranking of performance suggests that FGGAN and pix2pixHD provide state-of-the-art capabilities for SAR-to-optical translation, whereas AttenGAN and CycleGAN may be suitable in some contexts but lack robustness. PUT, however, likely requires further refinement before it can be applied to practical tasks requiring high structural fidelity.

Representative visual examples of these differences are shown in Figure 3. Differences between paired and unpaired image-to-image translation were observed in areas where grasslands and forests are adjacent, as shown in Figure 3. FGGAN and pix2pixHD achieved mean SSIM values above 0.98, with no substantial differences observed among the SAR datasets employed. In contrast, within unpaired image-to-image translation approaches, PUT demonstrated improvements in SSIM when using the H/A/Alpha decomposition or Yamaguchi’s four-component decomposition, rather than Gamma nought.

3.3 Spectral Bands

An examination of spectral band differences reveals consistent patterns across all SAR datasets and GAN models. As shown in Figure 2, the green band generally produces the highest SSIM values across most GAN architectures and SAR inputs. Generally, the green band produces the highest SSIM values, with both median and mean scores frequently exceeding those of the red and blue bands. This suggests that RGB reconstructions in the green channel retain the highest degree of structural similarity. The higher median positions of the green-band boxplots in Figure 2 support this observation, potentially because green wavelengths are more sensitive to vegetation and surface features, which are well captured by SAR data. The red band typically follows, producing slightly lower but still high SSIM values, indicating strong preservation of image structures with minor variability across models and datasets. In Figure 2, the red-band distributions appear slightly below the green-band distributions but remain tightly clustered, confirming stable performance. In contrast, the blue band consistently exhibits the lowest SSIM values, with wider variability reflected in lower minima and higher standard deviations. This is evident in Figure 2, where blue-band boxplots show larger spread and slightly lower medians across most models. This outcome suggests that blue-channel reconstructions present greater challenges for the GANs, possibly due to a weaker correlation between short-wavelength optical features and the scattering mechanisms captured by SAR data. Nevertheless, the blue band consistently maintains relatively high SSIM values (typically above 0.90 in median terms), underscoring the overall effectiveness of the models. These findings demonstrate that, while structural similarity is maintained across all bands, the performance hierarchy of green > red > blue remains consistent, as quantitatively demonstrated by the distributions in Figure 2, highlighting both the intrinsic spectral characteristics and the sensitivity of generative models to wavelength-dependent image features.

4. Discussion

The study area is primarily agricultural land, with major crops including beans, sugar beet, forage grasses, potatoes, wheat, and maize. In these environments, the dominant scattering mechanisms are strongly influenced by crop structure and

This contribution has been peer-reviewed. The double-blind peer-review was conducted on the basis of the full paper.
https://doi.org/10.5194/isprs-annals-XI-3-2026-797-2026

phenological stage. For example, broadleaf crops such as sugar beet and beans typically exhibit stronger volume scattering due to their dense canopies, whereas cereals such as wheat and maize can exhibit a combination of double-bounce scattering between stems and soil as well as volume scattering from leaves (Satalino et al., 2014; Sonobe et al., 2015). Forage grasses, by contrast, tend to produce relatively homogeneous backscatter dominated by surface and weak volume contributions (Bakhtiari and Zoughi, 1991; Lang, 1994).

The superior performance of PUT when using H/A/Alpha or Yamaguchi's decomposition may therefore be due to the richer representation of these scattering behaviours. H/A/Alpha provides explicit descriptors of entropy (scattering randomness), anisotropy, and the dominant scattering type, enabling effective discrimination between crops with distinct canopy structures. Similarly, Yamaguchi's four-component decomposition separates surface, double-bounce, volume, and helix scattering, capturing subtle variations associated with crop geometry and soil moisture. These additional polarimetric cues likely enhance the model's ability to reconstruct realistic RGB patterns that correspond closely to the optical appearance of different crop fields.

By contrast, the generalised Freeman–Durden decomposition, while useful for separating surface, double-bounce, and volume scattering, may not fully capture the diversity of agricultural scattering mechanisms, particularly in mixed cropping systems. This limitation may explain why its performance was comparable to that of simple Gamma nought backscatter, offering little added benefit in improving SSIM.

Moreover, unlike cropland, urban areas dominated by double-bounce scattering or open water characterised by strong surface scattering would likely highlight the advantages of polarimetric decompositions more clearly. In agricultural settings, however, the relative similarity of Freeman–Durden components to intensity-based backscatter reduces their discriminative value for RGB image generation.

5. Conclusion

This study demonstrated the feasibility of generating high-quality RGB images of agricultural areas using GANs trained on quad-pol SAR data from ALOS-2/PALSAR-2. A key contribution of this work is the systematic exploration of not only conventional backscatter coefficients (Gamma nought) but also polarimetric parameters derived from quad-pol data for RGB image synthesis. Our results showed that paired image-to-image translation architectures (e.g., FGGAN, pix2pixHD) consistently achieved high similarity to PlanetScope reference imagery, with mean SSIM values exceeding 0.98 across all SAR input types. By contrast, unpaired translation approaches exhibited more variable performance that depended strongly on the choice of polarimetric features. In particular, PUT benefitted significantly from H/A/Alpha and Yamaguchi's four-component decompositions, which provided enhanced structural and scattering information compared with Gamma nought alone. By contrast, the generalised Freeman–Durden decomposition produced results comparable to Gamma nought, suggesting limited additional benefit for cropland applications.

Overall, these findings highlight the potential of quad-pol SAR data not only as a reliable alternative to optical imagery in cloudy or low-light conditions but also as a valuable complementary data source, enriched through polarimetric decompositions. The ability to reconstruct realistic RGB images from polarimetric SAR data could contribute to more robust agricultural monitoring, especially in regions with frequent cloud cover. Future work will extend these analyses to a broader range of land-cover types, seasonal crop dynamics, and additional GAN frameworks to further assess the generality and applicability of this approach.

Future research could extend this work in several directions. First, the applicability of the proposed framework should be evaluated across different land-cover types beyond croplands, including urban areas and open water, where scattering mechanisms differ markedly. Second, temporal analyses using multi-seasonal SAR data should be conducted to provide insight into crop growth dynamics and to improve the robustness of GAN-based RGB reconstruction. Third, multisource data, such as Sentinel-1 SAR and Sentinel-2 optical imagery, should be integrated to enhance generalisability and to enable cross-sensor applications. Fourth, advanced generative models, including diffusion models or transformer-based architectures, should be explored to improve structural fidelity and spectral realism further. Finally, quantitative assessments of downstream tasks, such as crop classification or biomass estimation, should be performed to demonstrate the operational value of SAR-to-RGB translation for agricultural monitoring.

Acknowledgments

This work was supported by JSPS KAKENHI Grant Number 25K09353.

References

Bakhtiari, S., Zoughi, R., 1991: A model for backscattering characteristics of tall prairie grass canopies at microwave frequencies. *Remote Sens. Environ*., 36, 137-147. doi.org/10.1016/0034-4257(91)90036-6

Chen, X., Jia, C., 2021: An Overview of Image-to-Image Translation Using Generative Adversarial Networks, in: Lecture Notes in Computer Science (Including Subseries Lecture Notes in Artificial Intelligence and Lecture Notes in Bioinformatics). doi.org/10.1007/978-3-030-68780-9_31

Cloude, Shane., 2010: Polarisation: applications in remote sensing. Oxford University Press.

Dash, A., Ye, J., Wang, G., 2024: A Review of Generative Adversarial Networks (GANs) and Its Applications in a Wide Variety of Disciplines: From Medical to Remote Sensing. *IEEE Access* 12, 18330-18357. doi.org/10.1109/ACCESS.2023.3346273

Di Martino, G., Poderico, M., Poggi, G., Riccio, D., Verdoliva, L., 2012: SAR image simulation for the assessment of despeckling techniques, in: International Geoscience and Remote Sensing Symposium (IGARSS). doi.org/10.1109/IGARSS.2012.6351163

Goodfellow, I., Pouget-Abadie, J., Mirza, M., Xu, B., Warde-Farley, D., Ozair, S., Courville, A., Bengio, Y., 2020: Generative adversarial networks. *Commun ACM* 63, 139-144. doi.org/10.1145/3422622

Kamil, A., Shaikh, T., 2019: Literature Review of Generative models for Image-to-Image translation problems, in: Proceedings of 2019 International Conference on Computational Intelligence and Knowledge Economy, ICCIKE 2019. doi.org/10.1109/ICCIKE47802.2019.9004254

Lang, R.H., 1994: Microwave Backscattering and Emission Model for Grass Canopies. *IEEE Transactions on Geoscience and Remote Sensing* 32, 177-186. doi.org/10.1109/36.285200

Lee, J.-Sen., Pottier, Eric., 2009: Polarimetric radar imaging: from basics to applications. CRC Press.

Lin, Y., Zhang, S., Chen, T., Lu, Y., Li, G., Shi, Y., 2022: Exploring Negatives in Contrastive Learning for Unpaired Image-to-Image Translation, in: MM 2022 - Proceedings of the 30th ACM International Conference on Multimedia. doi.org/10.1145/3503161.3547802

Lopez-Sanchez, J.M., David Ballester-Berman, J., 2009: Potentials of polarimetric SAR interferometry for agriculture monitoring. *Radio Sci*. 44. doi.org/10.1029/2008RS004078

McNairn, H., Brisco, B., 2004: The application of C-band polarimetric SAR for agriculture: A review. *Canadian Journal of Remote Sensing* 30, 525-542. doi.org/10.5589/m03-069

McNairn, H., Shang, J., 2016: A review of multitemporal synthetic aperture radar (SAR) for crop monitoring, in: Remote Sensing and Digital Image Processing. doi.org/10.1007/978-3-319-47037-5_15

Pang, Y., Lin, J., Qin, T., Chen, Z., 2022: Image-to-Image Translation: Methods and Applications. I*EEE Trans Multimedia*. 24, 3859-3881. doi.org/10.1109/TMM.2021.3109419

Plank, S., Jussi, M., Martinis, S., Twele, A., 2017: Mapping of flooded vegetation by means of polarimetric Sentinel-1 and ALOS-2/PALSAR-2 imagery. *Int. J. Remote Sens.* 38, 3831-3850. doi.org/10.1080/01431161.2017.1306143

Rosenqvist, A., Shimada, M., Suzuki, S., Ohgushi, F., Tadono, T., Watanabe, M., Tsuzuku, K., Watanabe, T., Kamijo, S., Aoki, E., 2014: Operational performance of the ALOS global systematic acquisition strategy and observation plans for ALOS-2 PALSAR-2. *Remote Sens Environ* 155, 3-12. doi.org/10.1016/j.rse.2014.04.011

Satalino, G., Balenzano, A., Mattia, F., Davidson, M.W.J., 2014: C-band SAR data for mapping crops dominated by surface or volume scattering. *IEEE Geoscience and Remote Sensing Letters* 11, 384-388. doi.org/10.1109/LGRS.2013.2263034

Sonobe, R., 2019a: Combining ASNARO-2 XSAR HH and Sentinel-1 C-SAR VH/VV polarization data for improved crop mapping. *Remote Sens (Basel)* 11, 1920. doi.org/10.3390/rs11161920

Sonobe, R., 2019b: Parcel-based crop classification using multi-temporal TerraSAR-X dual polarimetric data. *Remote Sens (Basel)* 11, 1148. doi.org/10.3390/rs11101148

Sonobe, R., Tani, H., Shimamura, H., Mochizuki, K., 2024: Addition of fake imagery generated by generative adversarial networks for improving crop classification. *Advances in Space Research* 74, 2901-2914. doi.org/10.1016/j.asr.2024.06.026

Sonobe, R., Tani, H., Wang, X., Kobayashi, N., Shimamura, H., 2015: Discrimination of crop types with TerraSAR-X-derived information. *Physics and Chemistry of the Earth* 83-84. doi.org/10.1016/j.pce.2014.11.001

Sonobe, R., Tani, H., Zadi, M., Shimamura, H., Mochizuki, K., 2025: Improving crop classification accuracy using Sentinel-1 C-SAR data and GAN-generated optical images. *J Appl Remote Sens* 19, 024505. doi.org/10.1117/1.JRS.19.024505

Tang, H., Liu, H., Xu, D., Torr, P.H.S., Sebe, N., 2023: AttentionGAN: Unpaired Image-to-Image Translation Using Attention-Guided Generative Adversarial Networks. *IEEE Trans Neural Netw Learn Syst* 34, 1972-1987. doi.org/10.1109/TNNLS.2021.3105725

Tang, H., Xu, D., Sebe, N., Yan, Y., 2019: Attention-Guided Generative Adversarial Networks for Unsupervised Image-to-Image Translation, in: Proceedings of the International Joint Conference on Neural Networks. doi.org/10.1109/IJCNN.2019.8851881

Wang, T.C., Liu, M.Y., Zhu, J.Y., Tao, A., Kautz, J., Catanzaro, B., 2018: High-Resolution Image Synthesis and Semantic Manipulation with Conditional GANs, in: Proceedings of the IEEE Computer Society Conference on Computer Vision and Pattern Recognition. doi.org/10.1109/CVPR.2018.00917

Wang, Z., Bovik, A.C., Sheikh, H.R., Simoncelli, E.P., 2004: Image quality assessment: From error visibility to structural similarity. I*EEE Transactions on Image Processing* 13, 600-612. doi.org/10.1109/TIP.2003.819861

Wiseman, G., McNairn, H., Homayouni, S., Shang, J., 2014: RADARSAT-2 Polarimetric SAR response to crop biomass for agricultural production monitoring. *IEEE J Sel Top Appl Earth Obs Remote Sens* 7, 4461-4471. doi.org/10.1109/JSTARS.2014.2322311

Yamaguchi, Y., Moriyama, T., Ishido, M., Yamada, H., 2005: Four-component scattering model for polarimetric SAR image decomposition. *IEEE Transactions on Geoscience and Remote Sensing* 43, 1699-1706. doi.org/10.1109/TGRS.2005.852084

Yang, Y., Dan, X., Qiu, X., Gao, Z., 2020: FGGAN: Feature-Guiding Generative Adversarial Networks for Text Generation. *IEEE Access* 8, 105217-105225. doi.org/10.1109/ACCESS.2020.2993928

Zhu, J.Y., Park, T., Isola, P., Efros, A.A., 2017: Unpaired Image-to-Image Translation Using Cycle-Consistent Adversarial Networks, in: Proceedings of the IEEE International Conference on Computer Vision. doi.org/10.1109/ICCV.2017.244